Journal of Sol-Gel Science and Technology (2022) 104:558–565
https://doi.org/10.1007/s10971-022-05867-0

INVITED PAPER: NANO-STRUCTURED MATERIALS (PARTICLES, FIBERS, COLLOIDS, COMPOSITES, ETC.)

Fabrication of boehmite nanofiber aerogels by a phosphate gelation process for optical applications

Gen Hayase[1] · Keita Yamazaki[1,2] · Tetsuya Kodaira[3]

Received: 14 March 2022 / Accepted: 30 May 2022 / Published online: 20 July 2022

Abstract

A transparent wet gel was obtained in a few minutes at room temperature by adding an aqueous phosphoric acid solution of appropriate concentration to boehmite nanofiber sol. After room temperature aging and supercritical carbon dioxide drying, low bulk density aerogels with visible light transmittance of over 90% at 10 mm thickness were obtained. These aerogels exhibited high Young's modulus and visible light transmittance, while having the same bulk density as the samples obtained by a conventional gelation process using a base. The high optical transmittance of the aerogel were hardly lost even at high humidity because the phosphorylation of the skeletal surface reduced the percentage of hydroxyl groups. The three-dimensional imaging inspection of the exterior and interior of the aerogel was carried out. The various developments reported in this paper make aerogels with ultralow bulk density (<0.01 g cm^{-3}) and high visible light transmission even more promising for applications in the physical field.

Graphical abstract

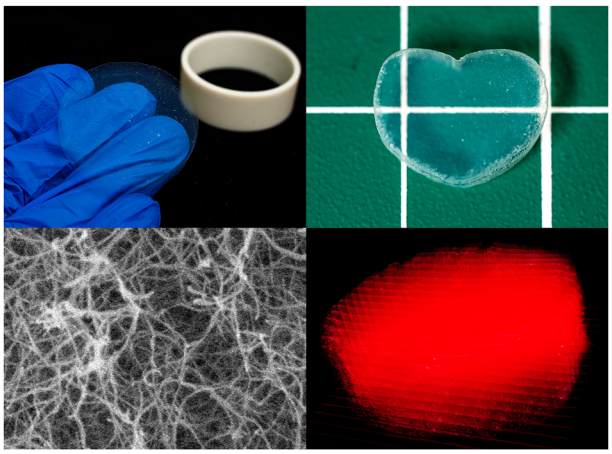

Keywords Aerogels · Porous materials · Nanofibers · Optical properties · Boehmite

Supplementary information The online version contains supplementary material available at https://doi.org/10.1007/s10971-022-05867-0.

✉ Gen Hayase
gen@aerogel.jp

[1] International Center for Materials Nanoarchitectonics, National Institute for Materials Science, 1-1 Namiki, Tsukuba, Ibaraki 305-0044, Japan

[2] Graduate School of Comprehensive Human Sciences, University of Tsukuba, 1-2 Kasuga, Tsukuba, Ibaraki 305-8550, Japan

[3] National Institute of Advanced Industrial Science and Technology (AIST), 1-1-1 Higashi, Tsukuba, Ibaraki 305-8565, Japan

Highlights

- Transparent gels were obtained by adding phosphoric acid to a boehmite nanofiber sol.
- Boehmite nanofiber aerogels with phosphate groups on the surface showed moisture resistance.
- The three-dimensional imaging inspection of the exterior and interior of the aerogel was carried out.

1 Introduction

Aerogels have fascinated researchers because of their characteristic properties derived from their low-density structures. A variety of aerogel materials have been reported [1], among which silica aerogel is the most representative one because of its high light transmittance and thermal insulation properties [2]. However, among porous materials with low bulk densities, not many skeletal compositions lead to high visible light transmittance. Organic polymer aerogels such as resorcinol-formaldehyde (RF) [3], polyimide [4] and polyurethane [5] have low light transmittance or are opaque, and carbon aerogels [6, 7] are black. On the other hand, bionanofiber gels, e.g. cellulose and chitosan nanofiber, which have attracted considerable research interest in recent years, are also translucent because of their tendency to cause Mie scattering [8, 9]. In fact, most of the aerogels that have been used as optical materials (detectors), for example, in accelerator experiments, are based on the silica framework [10–15].

In 2015, we reported the fabrication of aerogels using nanofibers with an aluminum oxide hydroxide (boehmite) framework [16]. Boehmite nanofiber (BNF) aerogels obtained by the gelation of an acetic acid-containing BNF suspension with the addition of a base, followed by washing and supercritical drying, have a minimum bulk density of ~1 mg cm^{-3}, which is comparable to or smaller than the lowest bulk density of a typical silica aerogel [17]. The skeletal network of the BNF aerogel is fiber-like and does not have interparticle necks like those observed in silica aerogel microstructures, and the BNF aerogel is mechanically strong in spite of its low bulk density [18]. In fact, it has a relatively high Young's modulus (>20kPa, with a sample of density ~5 mg cm^{-3}) against uniaxial compression and does not crack when crushed [19]. The disadvantage of using BNF aerogel as an optical material is that it tends to contain large defects caused by bubbles which tend to scatter a light beam [20]. The BNFs dispersed in the sol aggregate to form a gel when a base is added. However, if a basic salt or aqueous solution is added directly to the sol to induce its gelation, local aggregation occurs and a uniform aerogel cannot be obtained. Therefore, in a previous study, ammonia was generated in situ by the hydrolysis of hexamethylenetetramine (HMT) to induce the aggregation of the dispersed boehmite nanofibers for gelation. For the reaction to be efficient, the sol was heated to 60–80 °C. As the processing temperature was increased, the solubility of gas molecules decreased, and bubbles were more likely to form. Because the precursor sol contained a large number of nanofibers, it was difficult to completely suppress the nucleation and growth of air bubbles in the gelating mixture. In addition, BNF aerogels easily absorb moisture from air, resulting in a slight shrinkage and decrease in light transmittance with time after their fabrication.

After evaluating various gelation methods to resolve these issues, we discovered that the addition of phosphoric acid to a BNF sol could lead to uniform BNF monolithic gels without bubbles or aggregation. Simultaneously, aluminum phosphate formed on the nanofiber surface mitigated the moisture absorption by the aerogel. Herein, we report a new process involving phosphoric acid addition for fabricating transparent BNF aerogels for optical applications. In addition, differences between the gels obtained by the conventional gelation process with the addition of base will be discussed.

2 Experimental

2.1 Chemicals

Boehmite nanofiber (BNF) dispersion sol F1000 (7.5 wt.% in acetic acid aq.) was kindly provided by Kawaken Fine Chemicals Co., Ltd., Japan [21]. The concentration of nanofibers was confirmed by drying at 80 °C for 48 h. Average length and width of a BNF are 1400 and 4 nm, respectively. Aqueous phosphoric acid solution, methanol, 2-propanol, *n*-hexane, and hexamethylenetetramine (HMT) were purchased from Kanto Chemical Co. Inc., Japan. All the reagents were used as received.

2.2 Preparation of BNF aerogels

First, wet BNF gels were prepared using a phosphoric acid solution, as follows: x g of the BNF sol was diluted with $5.0 - x$ mL of ion-exchanged water in a perfluoroalkoxy alkane (PFA) container, and then 5.0 mL of 100 mM aq. phosphoric acid was added. After a few minutes of gelation, the gel was aged under sealed conditions for 24 h to obtain the wet gel. All these processes were carried out at RT. As a reference sample, a wet gel was formed by the addition of HMT using the following procedure: 1.0 g of the BNF sol was diluted with 9.0 mL of ion-exchanged water, and then

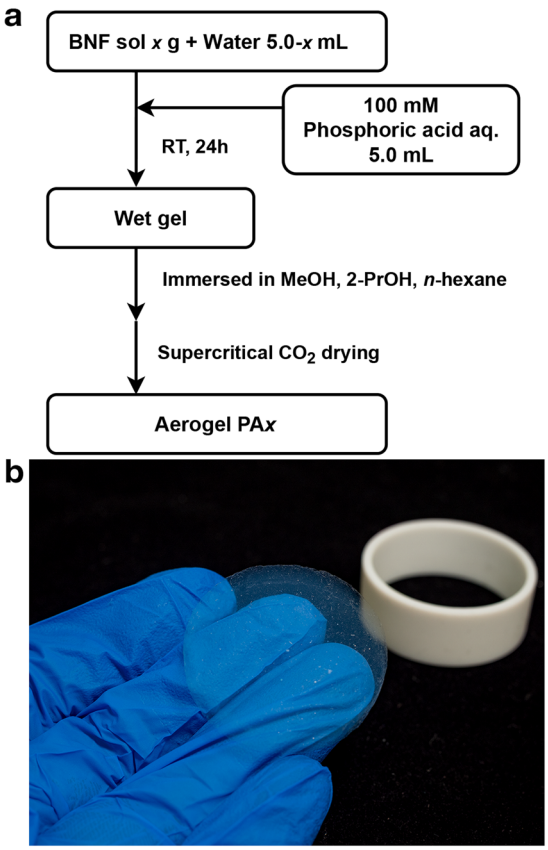

Fig. 1 Aerogel fabrication process and the sample obtained. **a** Flowchart for BNF aerogel PA*x* fabrication. **b** Disk sample of Aerogel PA1.0. The white object behind the sample is a polytetrafluoroethylene tube used as a mold for the gel

0.5 g of HMT was added and stirred for 3 min. After sonication and degassing for a few minutes, the sample was heated at 80 °C for 6 h under sealed conditions for gelation and aging. Thereafter, the two types of wet gels were washed and solvent-exchanged sequentially with methanol, 2-propanol, and *n*-hexane in that order. Finally, supercritical CO_2 drying was performed using SYGLCP-81 (Sanyu Gijutsu Co., Ltd., Japan). After solvent exchange of the samples to liquefied carbon dioxide in an autoclave, they were supercritically dried at 40 °C and 10 MPa. The sample prepared using aq. phosphoric acid is denoted as PA*x* (where $x = 0.5, 1.0, 1.5$), and the reference sample prepared with HMT is denoted as HMT1.0. A flowchart of the sample preparation process is presented in Fig. 1a.

2.3 Characterization

All aerogel samples were degassed under vacuum at 80 °C for 8 h before each measurement. The bulk densities were calculated based on the respective measured weights and volumes, with an error margin of ~5%. The microstructures were examined by scanning electron microscopy (SEM; SU8000, Hitachi High-Technologies Corp., Japan). The Al: P atomic ratios were determined using an energy-dispersive X-ray (EDX) spectrometer (Quantax FQ5060, Bruker, USA) attached to a scanning electron microscope. Uniaxial compression tests were performed on disk samples with a diameter of ~18 mm and height of ~6 mm using a mechanical tester (EZ-SX, Shimadzu Corp., Japan) with a 100 N pressure gauge. The Young's modulus was calculated from stress changes under compressive strains ranging from 2.5 to 5.0%. The visible light transmittance was analyzed using a spectrophotometer (C13555MA, Hamamatsu Photonics K.K., Japan) equipped with a halogen light source (KTX-100E, KenkoTokina Corporation, Japan) and an integrating sphere (HSU-O-DTR, Asahi Spectra Co., Ltd., Japan). The transmittance data were normalized to a thickness of 10 mm using the Lambert–Beer equation. Fourier transform infrared (FTIR) spectra were recorded using IRSpirit-L (Shimadzu Corp., Japan) with an attenuated total reflection (ATR) attachment QATR-S. A total of 100 scans were recorded at a resolution of 4 cm^{-1}. A SmartLab diffractometer (Rigaku Corp., Japan) with parallel beam geometry (Cu-K$\alpha_{1,2}$ radiation) was adopted for X-ray diffraction (XRD) measurements on samples in solid form. A parallel slit analyzer with an angle resolution of 0.5° and a pair of Soller slits of 2.5° were equipped for this measurement. For the moisture resistance test, aerogel samples were placed in a chamber and humidified air (relative humidity: ~100%) obtained by bubbling air in water was flown through the chamber at 5 L min^{-1} rate to evaluate the change in their appearance. Thermogravimetry-differential thermal analysis (TG-DTA) was performed using a Thermo Plus TG 8120 (Rigaku Corp., Japan) instrument at a heating rate of 5 °C min^{-1} with a dried air supply rate of 100 mL min^{-1}. The aerogels were imaged using a custom-built device consisting of a 1 mW red line laser ($\lambda = 635$ nm), a mechanical stage, and a digital camera (OM-D E-M5 Mark II, Olympus Corporation, Japan). The 0.5 mm spaced tomograms were reconstructed into a three-dimensional image using ImageJ2/Fiji and 3D Viewer plugin [22–24].

3 Results and discussion

3.1 Fabrication of BNF aerogels using the phosphate gelation method

Aqueous aluminum salt solutions generally produce transparent gel-like aggregates of aluminum hydroxide or aluminum phosphate when a weak base or phosphoric acid is added, respectively. Similarly, a sol of BNFs undergoes gelation with the addition of a base. We therefore speculated that a BNF gel could be obtained using phosphoric acid. We confirmed this by adding aq. phosphoric acid to a

Table 1 Physical properties of BNF aerogels

Sample	BNF sol in starting composition/g	Bulk density/ mg cm^{-3}	Young's modulus/ kPa	Transmittance at 550 nm/%
PA0.5	0.5	4.8	6.0	92.0
PA1.0	1.0	8.3	42.7	90.1
PA1.5	1.5	12.2	77.2	86.2
HMT1.0	–	8.3	20.2	86.5

diluted BNF sol and found that gelation occurred at phosphoric acid concentrations above ~15 mM. When the phosphoric acid concentration was varied gradually from 15 mM to 75 mM, the gelation time was the lowest at a phosphoric acid concentration of ~25 mM, and it became longer when the phosphoric acid concentration was increased slightly. This behavior is possibly due to the coexistence of acetate and phosphate anions in the sol, and a change in the compositional ratio of the aluminum salts, whose solubilities change with the pH change. At high concentrations of phosphoric acid of several hundered mM, gelation occurred instantly, as did with the addition of other strong acids such as hydrochloric acid. Through optimization, the gelation time was found to be a few minutes at ~50 mM, which is sufficient for uniform stirring. Therefore, the addition of ~50 mM phosphoric acid was selected as the optimal condition for further studies.

After supercritical drying, the wet BNF gel formed by phosphoric acid gelation yielded a transparent aerogel with a low bulk density (see the photograph in Fig. 1b), similar to that obtained by the gelation of the BNF sol using a base, i.e., HMT1.0. Table 1 presents the physical properties of the phosphate-based BNF aerogels (PA series) and HMT-based BNF aerogel (HMT1.0). For the PA series, the bulk density and Young's modulus increased with an increase in the number of nanofibers in the precursor sol, whereas the visible light transmittance decreased. This trend is common to the previously reported BNF aerogels. Both PA1.0 and HMT1.0 had almost the same bulk density, as they both shrank little during gelation, aging, and drying. However, Young's modulus and visible light transmittance (Fig. 2) were different. Scanning electron microscope observation of each sample revealed that the structure of PA1.0 was finer with less bundling of the BNFs than that of HMT1.0 (Fig. 3). In previous studies, BNFs were reported to be bundled by weak bases, but this was unlikely to occur with phosphate. [25]. The increased number of linkage points and reduced scattering sources due to a more dispersed nanofiber framework led to the PA1.0 aerogel's high Young's modulus and high visible light transmittance. In previous reports [19], BNF aerogels prepared with HMT were compressible without cracking, and PA1.0 showed similar properties (Fig. S1 in Supplementary Information (SI)).

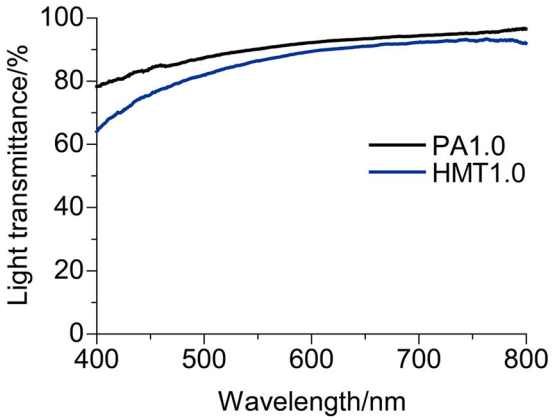

Fig. 2 Visible light transmittance of BNF aerogels

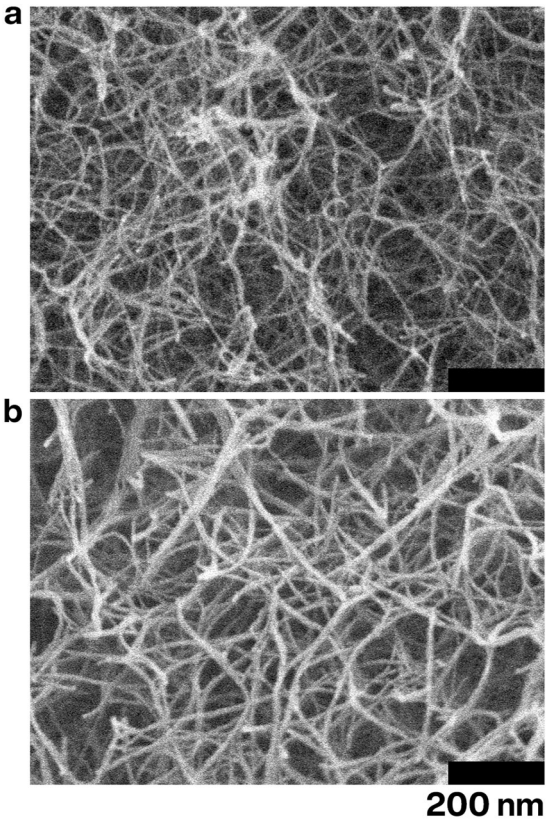

Fig. 3 SEM images of BNF aerogels. **a** PA1.0 and **b** HMT1.0

The change in the microstructure of the phosphate-based BNF aerogel can be attributed to the formation of aluminum phosphate on the surface of the nanofibers. The infrared spectrum of HMT1.0 obtained by the base gelation process was almost the same as that of the BNF solid obtained by drying the sol, whereas PA1.0 accompanies a broad absorption between 1300 and 950 cm^{-1} (Fig. 4). This is due to the P-O stretching vibrations at ~1135 and 1045 cm^{-1} owing to the reaction of the BNF with phosphoric acid. Meanwhile, the absorption peaks of the BNF (-OH bending

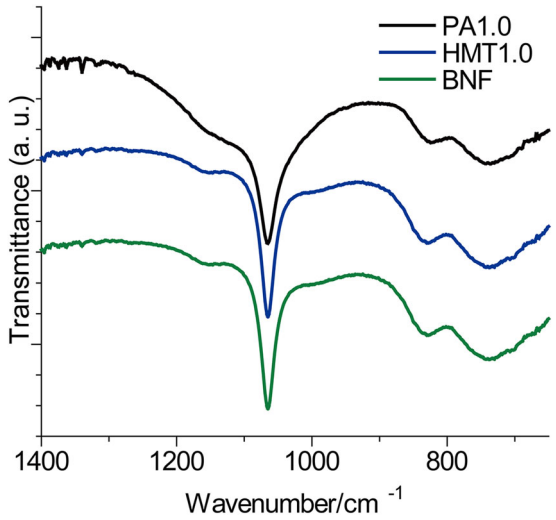

Fig. 4 Infrared spectra of BNF aerogels PA1.0, HMT1.0, and dried BNF

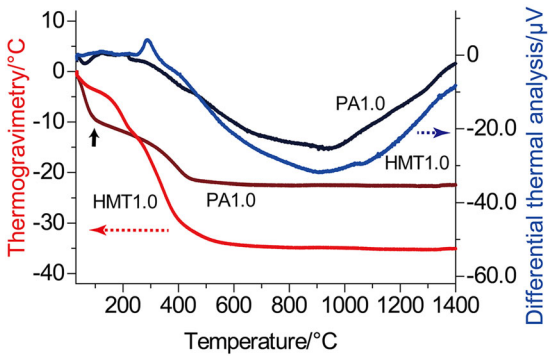

Fig. 5 Thermogravimetry-differential thermal curves for BNF aerogel PA1.0 and HMT1.0. In the PA1.0 sample, significant dehydration occurs below 100 °C (arrow)

vibrations of aluminum hydroxide) were observed at ~1160 and 1080 cm^{-1} [26, 27]. The Al:P ratio of the phosphate-based PA1.0 aerogel was determined to be 73:27 by EDX (Fig. S2 in SI). Although the hydroxyl groups of boehmite were not completely phosphorylated, the composition ratio and the crystal structure suggest that the reaction proceeds not only on the surface of the nanofibers, but also in the internal region. If the hydroxyl groups on the boehmite surface are consumed by phosphorylation, the formation of the Al-O-Al bond between nanofibers, which is generated by the dehydration of hydroxyl groups, will be prevented. This would prevent the bundling of nanofibers, resulting in the differences observed in the structures of PA1.0 and HMT1.0. In the XRD pattern, the full-width at half-maximum of each peak of PA1.0 was slightly larger than that of HMT1.0 (Fig. S3 in SI). The XRD results suggest that phosphorylation may have reduced the crystallite size of the boehmite phase and rendered the nanofibers thinner [28], which requires further investigations to confirm because the changes were subtle.

3.2 Moisture resistance of phosphate-based BNF aerogels

The HMT1.0 aerogel prepared by the reaction of the BNFs with the base derived from HMT gradually degrades due to moisture absorption and shrinks by up to 20% after a few days to a few months of storage in ambient conditions. This degradation not only causes dimensional instability, but also deteriorates the visible light transmittance and refractive index of the aerogel. This is a major obstacle to the use of BNF aerogels as optical materials. On the other hand, the reaction of the BNF with phosphoric acid decreases the number of hydroxyl groups on its surface, which could reduce the hygroscopicity and moisture-induced deterioration of the phosphate-based aerogels. When the samples were exposed to humidified air at room temperature and relative humidity of ~100%, HMT1.0 showed shrinkage and decrease in visible light transmittance, while PA1.0 showed no change in its appearance even after several days (Fig. S4 in SI). Moreover, no noticeable shrinkage occurred in PA1.0 for at least three months upon storing in ambient conditions of 20–22 °C and 40–60% relative humidity. These results indicate that the poor moisture resistance of the BNF aerogel was improved by the phosphate gelation process.

When the thermal changes in the BNF aerogels were examined by TG-DTA, a large difference was observed in the thermal weight change between PA1.0 and HMT1.0 (Fig. 5). The PA1.0 aerogel exhibited a large decrease in mass at 100 °C, followed by a smaller mass loss with increasing temperature. The decrease in mass at 1400 °C was ~22% for PA1.0 compared to 35% for HMT1.0. This difference in mass loss indicates that the phosphorylation of the hydroxyl groups of the BNFs facilitates the desorption of water physically adsorbed on the fiber surface and reduces the number of hydroxyl groups remaining in the nanofiber. In DTA, no clear difference was observed, except for the appearance of an exothermic peak for HMT1.0, possibly due to the oxidation of residual acetic acid. The heat resistance of BNF aerogels as a monolith was also investigated. Regardless of the gelation method, the aerogels remained transparent up to 800 °C. Because aluminum phosphate is thermally stable above 1400 °C, the temperature limit for both PA1.0 and HMT1.0 was the point at which γ-alumina (dehydrate of boehmite) undergoes a phase transition to θ-alumina.

3.3 Visual and internal inspection of BNF aerogels

The ratio of the solid phase to gas phase is a determining factor for the refractive index of an aerogel [29]. Bulk

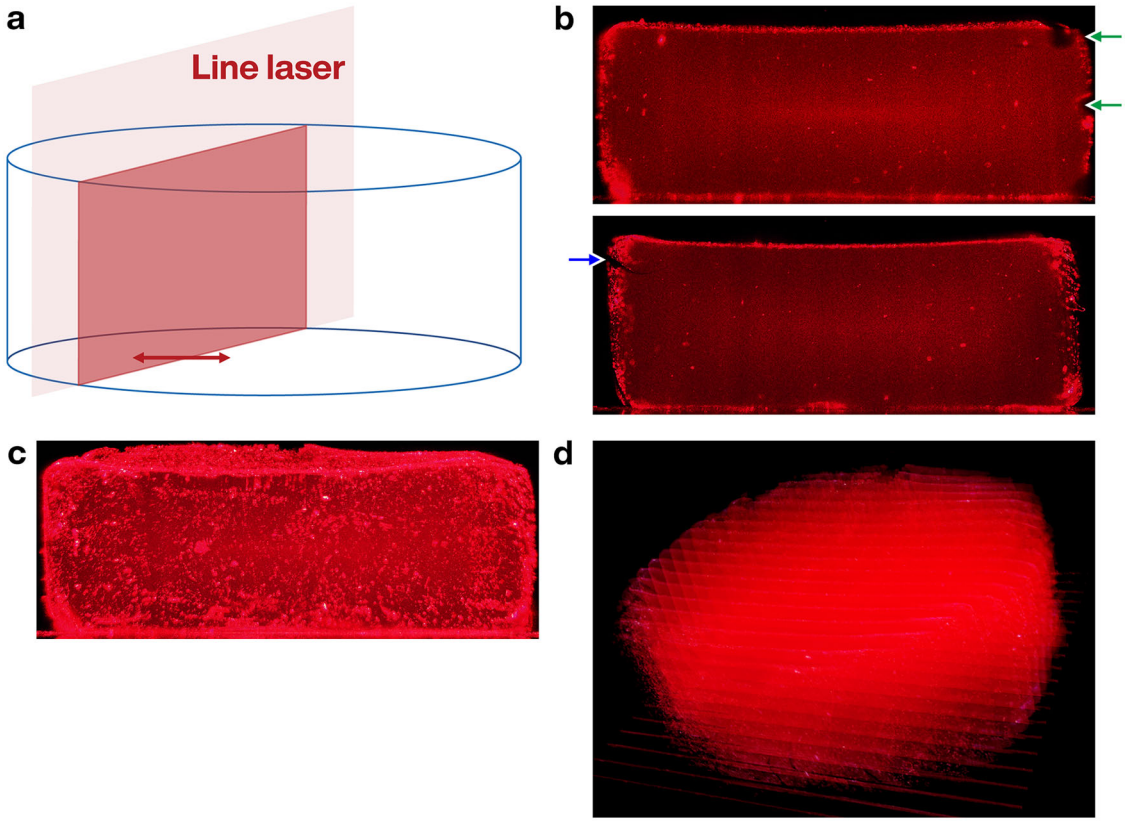

Fig. 6 Three-dimensional imaging inspection of BNF aerogel PA1.0. **a** Schematic of tomographic imaging. A red line laser with a wavelength of 635 nm was used as the light source. **b** Obtained tomographic image. The presence of bubbles can be seen in the upper image (green arrow) and cracks in the lower image (blue arrow). **c** Comparison bright composite image. By comparing multiple samples, the homogeneity can be relatively evaluated. **d** Three-dimensional reconstruction image obtained from tomograms at 0.5 mm intervals. The surface shape as well as the internal structure can be roughly evaluated

density is therefore an important parameter for the refractive index [30, 31]. As the BNF aerogel has ultralow bulk density, it hardly refracts light. This feature, together with visible light transmittance, is important for their application. When using aerogels for optical components, internal homogeneity is important. However, due to the optical properties, it is difficult to distinguish surface and internal deformations, cracks, and the inclusion of air bubbles with the naked eye. As colloids scatter light by the Tyndall's phenomenon when exposed to strong light, we used a line laser to illuminate a thin plane in the aerogel and obtained cross-sectional images for inspecting the external and internal features. Figure 6 shows the images and processed data obtained by illuminating the cross-section of the PA1.0 aerogel with a diameter of 18 mm at intervals of 0.5 mm. The presence of cracks and bubbles could be confirmed from the images of the slices (green and blue arrows in Fig. 6b, respectively), and the degree of aggregation or dust could be confirmed from the bright composite image (Fig. 6c). The three-dimensional reconstructed image clearly shows the internal and external features of the aerogel. This measurement can be only performed using a laser source, single-axis stage, and camera. In this study, manual measurements were performed, but automatic processing is also feasible owing to the simple configuration of the device.

Aerogels are known to be fragile and have poor processability. Because of the large differences in the skeletal morphologies, BNF aerogels are more susceptible to cracking and chipping under external forces than silica aerogels with the same bulk density. Therefore, it is difficult to reform them into a desired shape using mechanical processing after drying. In fact, the BNF aerogel collapsed when computer numerical control (CNC) micro milling was performed [32]. However, it was possible to fabricate a simple shape using a carbon dioxide laser (Fig. 7 and Movie S1 in SI). However, the resulting sample exhibited cloudiness on the cut surface, which was apparent even without the image inspection described above. This is due to the phase transition of alumina caused by the heat of laser irradiation. This issue can probably be overcome through nonthermal processing using a femtosecond laser [33], which we plan to study in the future.

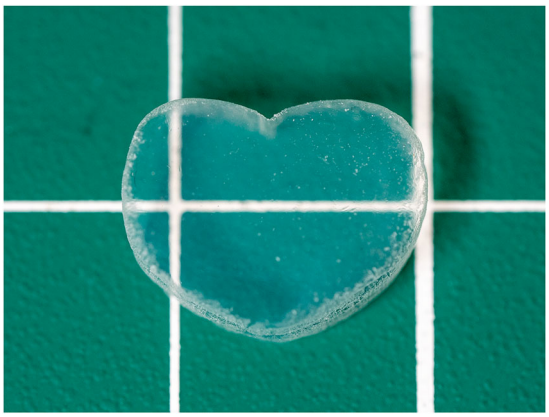

Fig. 7 Boehmite nanofiber aerogel PA1.0 cut into a heart shape using CO_2 laser. The processing is shown in MovieS1

4 Conclusion

A transparent wet gel of BNF was obtained in a few minutes at RT by adding an aqueous phosphoric acid solution at a concentration of 100 mM to a BNF suspension (sol). Then, through supercritical drying of the wet gel, an ultralow density transparent aerogel was obtained. The BNF aerogel exhibited high Young's modulus and visible light transmittance, while having the same bulk density as the samples obtained by a conventional gelation process using a base. The standard sample obtained in this study had a bulk density of 8.3 mg cm^{-3} and visible light transmittance of 90.1% ($\lambda = 550$ nm) at 10 mm thickness. Scanning electron microscope studies revealed that the microstructure of the aerogel became finer, and fewer bundles of nanofibers forming the skeleton. The differences in the physical properties and microstructure are speculated to be caused by the phosphorylation of hydroxyl groups on the surface and interior of the BNFs. A reduction in the number of hydroxyl groups decreases the probability of dehydration and chemisorption of water vapor. Consequently, the storage stability of the BNF aerogel improved significantly, even in a high humidity environment. The practicality of laser-based image inspection and processing for evaluating the suitability of the BNF aerogels as optical materials was also demonstrated.

Acknowledgements This work was supported by TIA collaborative research program and MEXT Leading Initiative for Excellent Young Researchers Grant.

Compliance with ethical standards

Conflict of interest The authors declare no competing interests.

References

1. Aegerter MA, Leventis N, Koebel MM (2011) Aerogels Handbook. Springer, New York
2. Hrubesh LW (1998) Aerogel applications. J Non-Cryst Solids 225:335–342. https://doi.org/10.1016/s0022-3093(98)00135-5
3. Pekala RW (1989) Organic aerogels from the polycondensation of resorcinol with formaldehyde. J Mater Sci 24:3221–3227. https://doi.org/10.1007/bf01139044
4. Meador MAB, Malow EJ, Silva R, Wright S, Quade D, Vivod SL, Guo HQ, Guo J, Cakmak M (2012) Mechanically strong, flexible polyimide aerogels cross-linked with aromatic triamine. ACS Appl Mater Interfaces 4:536–544. https://doi.org/10.1021/am2014635
5. Merillas B, Martin-de Leon J, Villafane F, Rodriguez-Perez MA (2021) Transparent polyisocyanurate-polyurethane-based aerogels: key aspects on the synthesis and their porous structures. ACS Appl Polym Mater 3:4607–4615. https://doi.org/10.1021/acsapm.1c00712
6. Lu X, Nilsson O, Fricke J, Pekala RW (1993) Thermal and electrical conductivity of monolithic carbon aerogels. J Appl Phys 73:581–584. https://doi.org/10.1063/1.353367
7. Merzbacher CI, Meier SR, Pierce JR, Korwin ML (2001) Carbon aerogels as broadband non-reflective materials. J Non-Cryst Solids 285:210–215. https://doi.org/10.1016/s0022-3093(01)00455-0
8. Takeshita S, Yoda S (2017) Translucent, hydrophobic, and mechanically tough aerogels constructed from trimethylsilylated chitosan nanofibers. Nanoscale 9:12311–12315. https://doi.org/10.1039/c7nr04051b
9. Kobayashi Y, Saito T, Isogai A (2014) Aerogels with 3D ordered nanofiber skeletons of liquid-crystalline nanocellulose derivatives as tough and transparent insulators. Angew Chem Int Ed 53:10394–10397. https://doi.org/10.1002/anie.201405123
10. Poelz G, Riethmuller R (1982) Preparation of silica aerogel for Cherenkov counters. Nucl Instrum Methods Phys Res 195:491–503. https://doi.org/10.1016/0029-554x(82)90010-6
11. Cantin M, Casse M, Koch L, Jouan R, Mestreau P, Roussel D, Bonnin F, Moutel J, Teichner SJ (1974) Silica aerogels used as cherenkov radiators. Nucl Instrum Methods 118:177–182. https://doi.org/10.1016/0029-554x(74)90700-9
12. Sumiyoshi T, Adachi I, Enomoto R, Iijima T, Suda R, Yokoyama M, Yokogawa H (1998) Silica aerogels in high energy physics. J Non-Cryst Solids 225:369–374. https://doi.org/10.1016/s0022-3093(98)00057-x
13. Hotaling SP (1993) Ultra-low density aerogel optical applications. J Mater Res 8:352–355. https://doi.org/10.1557/jmr.1993.0352
14. Plata DL, Briones YJ, Wolfe RL, Carroll MK, Bakrania SD, Mandel SG, Anderson AM (2004) Aerogel-platform optical sensors for oxygen gas. J Non-Cryst Solids 350:326–335. https://doi.org/10.1016/j.jnoncrysol.2004.06.046
15. Morris CA, Anderson ML, Stroud RM, Merzbacher CI, Rolison DR (1999) Silica sol as a nanoglue: flexible synthesis of composite aerogels. Science 284:622–624. https://doi.org/10.1126/science.284.5414.622
16. Hayase G, Nonomura K, Hasegawa G, Kanamori K, Nakanishi K (2015) Ultralow-density, transparent, superamphiphobic boehmite nanofiber aerogels and their alumina derivatives. Chem Mater 27:3–5. https://doi.org/10.1021/cm503993n
17. Tillotson TM, Hrubesh LW (1992) Transparent ultralow-density silica aerogels prepared by a 2-step sol-gel process. J Non-Cryst Solids 145:44–50. https://doi.org/10.1016/s0022-3093(05)80427-2
18. Hæreid S, Anderson J, Einarsrud MA, Hua DW, Smith DM (1995) Thermal and temporal aging of TMOS-based aerogel precursors in water. J Non-Cryst Solids 185:221–226

19. Hayase G (2021) Boehmite nanofiber-polymethylsilsesquioxane composite aerogels: synthesis, analysis, and thermal conductivity control via compression processing. Bull Chem Soc Jpn 94:70–75. https://doi.org/10.1246/bcsj.20200205
20. Hayase G, Funatomi T, Kumagai K (2018) Ultralow-bulk-density transparent boehmite nanofiber cryogel monoliths and their optical properties for a volumetric three-dimensional display. ACS Appl Nano Mater 1:26–30. https://doi.org/10.1021/acsanm.7b00097
21. Nagai N, Mizukami F (2011) Properties of Boehmite and Al_2O_3 thin films prepared from boehmite nanofibres. J Mater Chem 21:14884–14889. https://doi.org/10.1039/c1jm11571e
22. Rueden CT, Schindelin J, Hiner MC, DeZonia BE, Walter AE, Arena ET, Eliceiri KW (2017) ImageJ2: ImageJ for the next generation of scientific image data. BMC Bioinform 18:529. https://doi.org/10.1186/s12859-017-1934-z
23. Schmid B, Schindelin J, Cardona A, Longair M, Heisenberg M (2010) A high-level 3D visualization API for Java and ImageJ. BMC Bioinform. 11: https://doi.org/10.1186/1471-2105-11-274
24. Schindelin J, Arganda-Carreras I, Frise E, Kaynig V, Longair M, Pietzsch T, Preibisch S, Rueden C, Saalfeld S, Schmid B, Tinevez JY, White DJ, Hartenstein V, Eliceiri K, Tomancak P, Cardona A (2012) Fiji: an open-source platform for biological-image analysis. Nat Methods 9:676–682. https://doi.org/10.1038/nmeth.2019
25. Kodaira T, Suzuki Y-h, Nagai N, Matsuda G, Mizukami F (2015) A highly photoreflective and heat-insulating alumina film composed of stacked mesoporous layers in hierarchical structure. Adv Mater 27:5901–5905. https://doi.org/10.1002/adma.201502064
26. Watanabe Y, Kasama T, Fukushi K, Ikoma T, Komatsu Y, Tanaka J, Moriyoshi Y, Yamada H (2011) Synthesis of nano-sized boehmites for optimum phosphate sorption. Sep Sci Technol 46:818–824. https://doi.org/10.1080/01496395.2010.535590
27. Kiss AB, Keresztury G, Farkas L (1980) Raman and I.R. spectra and structure of Boehmite (γ-AlOOH). Evidence for the recently discarded D^17_2H space group. Spectrochim Acta A 36:653–658. https://doi.org/10.1016/0584-8539(80)80024-9
28. Mathieu Y, Lebeau B, Valtchev V (2007) Control of the morphology and particle size of boehmite nanoparticles synthesized under hydrothermal conditions. Langmuir 23:9435–9442. https://doi.org/10.1021/la700233q
29. Wang P, Beck A, Korner W, Scheller H, Fricke J (1994) Density & refractive-index of silica aerogels after low-temperature and high-temperature supercritical drying and thermal-treatment. J Phys D: Appl Phys 27:414–418. https://doi.org/10.1088/0022-3727/27/2/036
30. Buzykaev AR, Danilyuk AF, Ganzhur SF, Kravchenko EA, Onuchin AP (1999) Measurement of optical parameters of aerogel. Nucl Instrum Methods Phys Res, Sect A 433:396–400. https://doi.org/10.1016/s0168-9002(99)00325-3
31. Emmerling A, Petricevic R, Beck A, Wang P, Scheller H, Fricke J (1995) Relationship between optical transparency and nanostructural features of silica aerogels. J Non-Cryst Solids 185:240–248. https://doi.org/10.1016/0022-3093(95)00021-6
32. Balazs BZ, Geier N, Takacs M, Davim JP (2021) A review on micro-milling: recent advances and future trends. Int J Adv Manuf Technol 112:655–684. https://doi.org/10.1007/s00170-020-06445-w
33. Sun J, Longtin JP, Norris PM (2001) Ultrafast laser micromachining of silica aerogels. J Non-Cryst Solids 281:39–47. https://doi.org/10.1016/s0022-3093(00)00426-9